



Molecular beam epitaxy of $\text{Co}_x\text{Fe}_{4-x}\text{N}$ ($0.4 < x < 2.9$) thin films on $\text{SrTiO}_3(001)$ substrates

| | |
|------------------------------|--|
| 著者 | Sanai Tatsunori, Ito Keita, Toko Kaoru, Suemasu Takashi |
| journal or publication title | Journal of crystal growth |
| volume | 357 |
| page range | 53-57 |
| year | 2012-10 |
| 権利 | (C) 2012 Elsevier B.V. NOTICE: this is the author's version of a work that was accepted for publication in Journal of crystal growth. Changes resulting from the publishing process, such as peer review, editing, corrections, structural formatting, and other quality control mechanisms may not be reflected in this document. Changes may have been made to this work since it was submitted for publication. A definitive version was subsequently published in Journal of crystal growth, Volume 357, 2012, DOI:10.1016/j.jcrysgro.2012.07.032. |
| URL | http://hdl.handle.net/2241/117637 |

doi: 10.1016/j.jcrysgro.2012.07.032

1 **Molecular beam epitaxy of $\text{Co}_x\text{Fe}_{4-x}\text{N}$ ($0.4 < x < 2.9$) thin films on $\text{SrTiO}_3(001)$ substrates**

3 Tatsunori Sanai, Keita Ito, Kaoru Toko, Takashi Suemasu

4 *Institute of Applied Physics, Graduate School of Pure and Applied Sciences, University of*

5 *Tsukuba, 1-1-1 Tennohdai, Tsukuba, Ibaraki 305-8573, Japan*

7 **Abstract**

8 We attempted to grow $\text{Co}_x\text{Fe}_{4-x}\text{N}$ epitaxial thin films on $\text{SrTiO}_3(001)$ substrates by molecular
9 beam epitaxy supplying solid Co and Fe and a radio frequency N_2 plasma, simultaneously.

10 The composition ratio of Co/Fe in $\text{Co}_x\text{Fe}_{4-x}\text{N}$ was controlled by changing the weight ratio of
11 Co to Fe flakes in the crucible of the Knudsen cell used. We confirmed epitaxial growth of
12 $\text{Co}_x\text{Fe}_{4-x}\text{N}$ ($0.4 < x < 2.9$) thin films by reflection high-energy electron diffraction and θ - 2θ
13 X-ray diffraction patterns. The in-plane lattice parameter of the $\text{Co}_x\text{Fe}_{4-x}\text{N}$ films was almost
14 the same as the out-of-plane lattice parameter, and they decreased with increasing Co
15 composition, following Vegard's law.

17 *Keywords:* A3.Molecular beam epitaxy, B2.Ferromagnetic materials, B1. $\text{Co}_x\text{Fe}_{4-x}\text{N}$,
18 B1. SrTiO_3

1. Introduction

Highly spin-polarized ferromagnetic materials have attracted increasing attention for high-performance spintronics devices such as the read heads of hard disc drives and spin random access memory. For these materials, special attention has been focused on cubic perovskite 3d ferromagnetic nitrides such as Fe_4N and Co_4N . The spin asymmetry $\beta = (\sigma_{\uparrow} - \sigma_{\downarrow})/(\sigma_{\uparrow} + \sigma_{\downarrow})$ of Fe_4N was calculated to be -1.0 [1], and we evaluated $|\beta|$ to be 0.59 at 7.8 K by means of point contact Andreev reflection measurement [2]. There have been a few reports on the inverse tunnel magnetoresistance of -75% in $\text{CoFeB/MgO/Fe}_4\text{N}$ magnetic tunnel junctions and negative anisotropic magnetoresistance in Fe_4N films at room temperature [3-6]. The spin-resolved density of states (D) in Co_4N was calculated [7,8], and spin polarization $P = (D_{\uparrow} - D_{\downarrow})/(D_{\uparrow} + D_{\downarrow})$ at the Fermi level was estimated to be -0.88 by Imai *et al.*, which exceeds that in Fe_4N of -0.67 [8]. We have already succeeded in epitaxial growth of Fe_4N and Co_4N thin films on $\text{SrTiO}_3(\text{STO})(001)$ substrates by molecular beam epitaxy (MBE) [9,10] and we evaluated the spin and orbital magnetic moments by X-ray magnetic circular dichroism [11,12]. Recent first-principles calculation indicating that P was estimated to be -1.0 in Co_3FeN has renewed interest in this material [13]. There have been several reports on perovskite mixed crystal nitrides such as $(\text{Co,Fe})_4\text{N}$ and $(\text{Mn,Fe})_4\text{N}$. H. Y. Wang *et al.* formed CoFeN films by radio frequency (RF) magnetron sputtering and evaluated their magnetic anisotropy [14-16]. First-principles calculations were performed for the electronic and

magnetic structures in $(\text{Mn,Fe})_4\text{N}$ [17-20]. D. L. Peng *et al.* characterized perpendicular magnetic anisotropy of $(\text{Fe,Cr})_4\text{N}_x$ films formed by DC magnetron sputtering [21-23]. However, there have been no reports so far on epitaxial growth of $(\text{Co,Fe})_4\text{N}$ thin films. In order to apply $(\text{Co,Fe})_4\text{N}$ films to spintronics devices, characterization of the basic material properties of high quality $(\text{Co,Fe})_4\text{N}$ films is required. In this study, we attempted to grow $(\text{Co,Fe})_4\text{N}$ epitaxial films on STO(001) substrates by MBE, while varying the composition ratio of Co/Fe in $(\text{Co,Fe})_4\text{N}$.

2. Experimental procedures

Approximately 25-nm-thick $(\text{Co,Fe})_4\text{N}$ thin films were grown on STO(001) substrates by supplying Co, Fe and N atoms simultaneously using an ion-pumped MBE system equipped with a high-temperature Knudsen cell for Co and Fe, and an RF- N_2 plasma for N [9,10]. The lattice mismatch between Fe_4N and STO is 2.8%, and that between Co_4N and STO is 4.3%. Co and Fe flakes were placed into the same crucible. Various weight ratios of Co/Fe in the crucible were used including 0.5:1 (sample A), 1:1 (sample B), 3:1 (sample C) and 5.6:1 (sample D). During the growth of these samples, the temperature of the STO substrate was kept at 450 °C, and the deposition rate of Co plus Fe was set to be approximately 0.5 nm/min. The flow rate of the N_2 gas was fixed at 1.0 sccm, and the input power to the RF plasma was 140 W. The pressure inside the chamber was approximately 1×10^{-4} Torr during film growth.

The crystalline quality of samples A-D was evaluated by reflection high-energy electron diffraction (RHEED) and θ - 2θ X-ray diffraction (XRD). We deduced the lattice constants of samples along directions perpendicular and parallel to the substrate surface from out-of-plane and in-plane θ - 2θ XRD patterns, respectively. The composition ratio of Co/Fe in the films was determined by energy dispersive X-ray spectroscopy (EDX) using an accelerating voltage of 10 kV with a spot size of 30 μm and by Rutherford back scattering spectrometry (RBS) using a He ion beam with an acceleration voltage of 2.3 MeV.

3. Results and discussion

Figures 1(a)-1(d) show the RHEED patterns of samples A-D, respectively. Streaky RHEED patterns were obtained except for the spotty pattern for sample B. Figure 2(a) shows the out-of-plane θ - 2θ XRD patterns of $\text{Fe}_4\text{N}/\text{STO}(001)$, and Figs. 2(b)-2(e) show those of samples A-D, respectively. In samples A-D, the diffraction peaks of $(\text{Co,Fe})_4\text{N}(001)$, (002) and (004) were observed. With increasing weight ratio of Co to Fe in the crucible, these peaks shifted to a higher angle. Figures 3(a)-3(d) show the in-plane θ - 2θ XRD patterns of samples A-D around $2\theta=23^\circ$, respectively. The diffraction peaks of $(\text{Co,Fe})_4\text{N}(100)$ were clearly observed in these samples. With increasing weight ratio of Co to Fe in the crucible, these peaks also shifted to a higher angle. According to the X-ray extinction law, the diffraction peak of fcc-Co(100) is forbidden; however, that of $(\text{Co,Fe})_4\text{N}(100)$ is allowed.

The experimentally obtained intensity ratios of (100) to (200) were 0.0096, 0.0092, 0.0074, and 0.0079, in samples A-D, respectively. In the case of Co_4N , the intensity ratio is theoretically estimated to be 0.027. Therefore, we can state that the grown layers are not fcc-Co, but $(\text{Co,Fe})_4\text{N}$ in which N atom is located at the body center of the unit cell. On the basis of these results, we confirmed that the $(\text{Co,Fe})_4\text{N}$ layers grew epitaxially on the STO(001) substrates. At present, we cannot determine the degree of order of N atoms. It can be estimated, for example, by comparing the experimentally obtained intensity ratios of (100) to (200) with theoretical ones. However, information about Fe and Co sites in the unit cell of $(\text{Co,Fe})_4\text{N}$ is limited at present, and thus further studies are mandatory for this estimation. A small diffraction peak of Fe(002) in Figs. 2(b)-2(e) indicate that pure Fe exists in the $(\text{Co,Fe})_4\text{N}$ layers of samples A-D. However, the peak intensities were negligibly small compared to those of $(\text{Co,Fe})_4\text{N}$. Thus, we consider that the analysis of the composition ratio Co/Fe in the $(\text{Co,Fe})_4\text{N}$ layers of samples A-D was not affected by the existence of pure Fe, if there was any present. In order to determine the Co/Fe composition ratio in the $(\text{Co,Fe})_4\text{N}$ layers using EDX measurements, we grew an Au(5 nm)/ $(\text{Co,Fe})_4\text{N}$ (12 nm) film on the MgO(001) substrate (sample E) using the same growth procedure as sample C, and evaluated the composition ratio of Co, Fe and N using RBS measurements.

Figure 4 shows the RBS depth profiles of Co, Fe, N, Au, Mg and O atoms in sample E. The composition ratio in the $(\text{Co,Fe})_4\text{N}$ layer was evaluated to be approximately Co:Fe =

1.4:1.0, and (Co+Fe):N = 4:1. We assumed that the composition ratio of (Co,Fe)₄N in sample C was the same as that in sample E, and we estimated the Co/Fe ratio in sample C to be Co_{2.3}Fe_{1.7}N. Figures 5(a)-5(d) show the EDX spectra of samples A-D, respectively. Peaks of Co K_{α} (6.924 keV) and Fe K_{β} (7.057 keV) X-rays partially overlapped. We separated the overlapped peak into two peaks using Gaussian curve fitting. The integrated intensity of the Co K_{α} X-ray peak was enhanced with increasing weight ratio of Co/Fe in the crucible. On the other hand, the integrated intensity of the Fe K_{α} X-ray peak was relatively suppressed. We determined the composition ratio in the (Co,Fe)₄N layers of samples A, B and D using the RBS measurements for sample E and obtained EDX spectra of samples A-D. First, we deduced a constant value γ using

$$\frac{EDX_{CoK\alpha}}{EDX_{FeK\alpha}} = \gamma \frac{RBS_{Co}}{RBS_{Fe}}, \quad (1)$$

where $EDX_{CoK\alpha} / EDX_{FeK\alpha}$ is the ratio of integrated EDX intensity of Co K_{α} to Fe K_{α} X-rays in sample C, and RBS_{Co} / RBS_{Fe} is the composition ratio of Co/Fe in sample E obtained by the RBS depth profiles shown in Fig. 4. We evaluated the composition ratio of Co/Fe in (Co,Fe)₄N layers for samples A, B and D using $EDX_{CoK\alpha} / EDX_{FeK\alpha}$ of these samples divided by the constant γ to be Co_{0.4}Fe_{3.6}N, Co_{1.2}Fe_{2.8}N and Co_{2.9}Fe_{1.1}N, respectively, as summarized in Table 1.

Figure 6(a) shows the out-of-plan lattice constants of samples A-D deduced from (Co,Fe)₄N(002) and (Co,Fe)₄N(004) θ -2 θ XRD peak positions plotted as a function of $\cot\theta$.

The peak positions were determined by Gaussian fitting for the XRD patterns, and lattice constants were deduced by Bragg's law. Figure 6(b) shows the out-of-plane lattice constants of samples A-D after correction of the measurement error, by extrapolating from the intersection of the straight line passing through the above two points at $\cot\theta = 0$ in Fig. 5(a), plotted against the composition ratio of $\text{Co}_x\text{Fe}_{4-x}\text{N}$. A dashed line is drawn for Vegard's law [24] using the bulk lattice constants of Fe_4N (0.3796 nm) [25] and Co_4N (0.3738 nm) [26]. The out-of-plane lattice constants of samples A-D were 0.3793, 0.3768, 0.3761 and 0.3750 nm, respectively. Figures 7(a)-7(b) show the case of in-plane θ - 2θ XRD measurements. In-plane lattice constants for samples A-D were deduced to be 0.3788, 0.3775, 0.3755 and 0.3737 nm, respectively, using the same method as the out-of-plane case. Both out-of-plane and in-plane lattice constants decreased with increasing Co/Fe ratio in $\text{Co}_x\text{Fe}_{4-x}\text{N}$, and they followed Vegard's law. There was no significant difference between out-of-plane and in-plane lattice constants, indicating that the lattice was almost strain-free.

4. Conclusions

We have succeeded in growing $\text{Co}_x\text{Fe}_{4-x}\text{N}$ ($0.4 < x < 2.9$) thin films epitaxially on STO(001) substrates by MBE supplying solid Co, Fe, and RF- N_2 , simultaneously. We were able to control the composition ratio of Co/Fe in $(\text{Co,Fe})_4\text{N}$ by changing the weight ratio of Co to Fe flakes in the crucible. The lattice constants of the grown films decreased with

134 increasing Co/Fe ratio, and they were in good agreement with Vegard's law. We also
135 confirmed that the lattice was almost relaxed in the 25-nm-thick (Co,Fe)₄N films on
136 STO(001).

137

138 **Acknowledgements**

139 In-plane XRD measurements were performed with the help of Dr. Y. K. Takahashi,
140 Dr. T. Furubayashi and Prof. K. Hono of the National Institute for Materials Science (NIMS),
141 Tsukuba and the Rigaku Corporation. The authors thank Dr. Y. Imai of the National Institute
142 of Advanced Industrial Science and Technology (AIST), Tsukuba, for useful discussions.

143

144 **References**

- 145 [1] S. Kokado, N. Fujima, K. Harigaya, H. Shimuzu, A. Sakuma, Phys. Rev. B **73** (2006)
146 172410.
- 147 [2] A. Narahara, K. Ito, T. Suemasu, Y. K. Takahashi, A. Rajanikanth, K. Hono, Appl. Phys.
148 Lett. **94** (2009) 202502.
- 149 [3] Y. Komasaki, M. Tsunoda, S. Isogami, M. Takahashi, J. Appl. Phys. **105** (2009) 07C928.
- 150 [4] M. Tsunoda, Y. Komasaki, S. Kokado, S. Isogami, C. C. Chen, M. Takahashi, Appl. Phys.
151 Express **2** (2009) 083001.
- 152 [5] M. Tsunoda, H. Takahashi, S. Kokado, Y. Komasaki, A. Sakuma, M. Takahashi, Appl.
153 Phys. Express **3** (2010) 113003.
- 154 [6] K. Ito, K. Kabara, H. Takahashi, T. Sanai, K. Toko, T. Suemasu, M. Tsunoda, Jpn. J. Appl.
155 Phys. **51** (2012) 068001.
- 156 [7] S. F. Mater, A. Houari, M. A. Belkhir, Phys. Rev. B **75** (2007) 245109.
- 157 [8] Y. Imai, Y. Takahashi, T. Kumagai, J. Magn. Magn. Mater. **322** (2010) 2665.
- 158 [9] K. Ito, G. H. Lee, H. Akinaga, T. Suemasu, J. Cryst. Growth **322** (2011) 63.
- 159 [10] K. Ito, K. Harada, K. Toko, H. Akinaga, T. Suemasu, J. Cryst. Growth **336** (2011) 40.
- 160 [11] K. Ito, G. H. Lee, K. Harada, M. Suzuno, T. Suemasu, Y. Takeda, Y. Saitoh, M. Ye, A.
161 Kimura, H. Akinaga, Appl. Phys. Lett. **98** (2011) 102507.
- 162 [12] K. Ito, K. Harada, K. Toko, M. Ye, A. Kimura, Y. Takeda, Y. Saitoh, H. Akinaga, T.

163 Suemasu, Appl. Phys. Lett. **99** (2011) 252501.

164 [13] Y. Takahashi, Y. Imai, T. Kumagai, J. Magn. Magn. Mater. **322** (2011) 2941.

165 [14] H. Y. Wang, E. Y. Jiang, Z. W. Ma, Y. J. He, H. S. Huang, J. Phys. Condens. Matter. **11**

166 (1999) 989.

167 [15] K. K. Shih, J. Karasinski, J. Appl. Phys. **73** (1993) 8377.

168 [16] N. D. Ha, B. C. Parka, H. B. Kima, C. G. Kima, C. O. Kim, J. Magn. Magn. Mater. **286**

169 (2005) 267.

170 [17] C. A. Kuhnen, A. V. dos Santos, J. Magn. Magn. Mater. **130** (1994) 353.

171 [18] C. Paduani, J. Appl. Phys. **96** (2004) 1503.

172 [19] M. S. Patwari, R. H. Victora, Phys. Rev. B **64** (2001) 214417.

173 [20] L. Chen, J. Appl. Phys. **100** (2006) 113717.

174 [21] D. L. Peng, K. Sumiyama, T. J. Konno, K. Suzuki, Jpn. J. Appl. Phys. **36** (1997) L479.

175 [22] D. L. Peng, T. J. Konno, K. Sumiyama, H. Onodera, K. Suzuki, J. Magn. Magn. Mater.

176 **172** (1997) 41.

177 [23] D. L. Peng, K. Sumiyama, K. Suzuki, J. Alloys Compd. **265** (1998) 49.

178 [24] L. Vegard, Z. Phys. **5** (1921) 17.

179 [25] H. Jacobs, D. Rechenbach, U. Zachwieja, J. Alloys Compd. **227** (1995) 10.

180 [26] N. Terao, Mem. Sci. Rev. Met. **57** (1960) 96.

181

182 **Figs. 1.** RHEED patterns of samples A-D along the azimuths of the STO[100] direction.

183

184 **Fig. 2.** Out-of-plane θ - 2θ XRD patterns of Fe₄N and samples A-D.

185

186 **Fig. 3.** In-plane θ - 2θ XRD patterns of samples A-D around $2\theta=23^\circ$.

187

188 **Fig. 4.** RBS depth profiles of Co, Fe, N, Au, Mg and O atoms in sample E.

189

190 **Fig. 5.** EDX spectra of samples A-D.

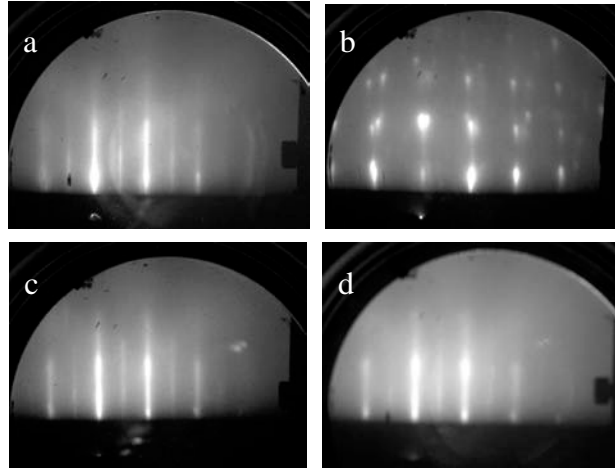
191

192 **Figs. 6.** (a) Out-of-plane lattice constants of samples A-D deduced from XRD peak positions
193 plotted as a function of $\cot\theta$. (b) Corrected out-of-plane lattice constants plotted as a function
194 of the composition ratio of Co_xFe_{4-x}N.

195

196 **Figs. 7.** (a) In-plane lattice constants of samples A-D deduced from XRD peak positions
197 plotted as a function of $\cot\theta$. (b) Corrected in-plane lattice constants plotted as a function of
198 the composition ratio of Co_xFe_{4-x}N.

199



Figs. 1

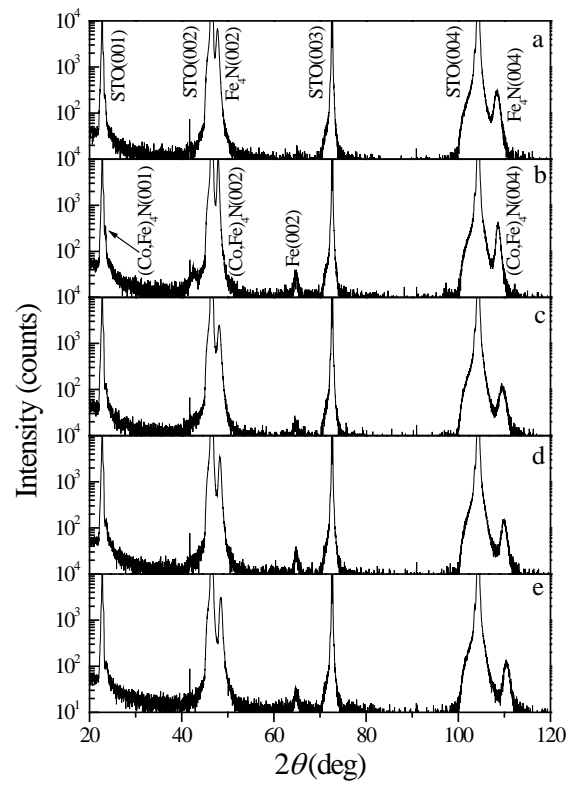


Fig. 2

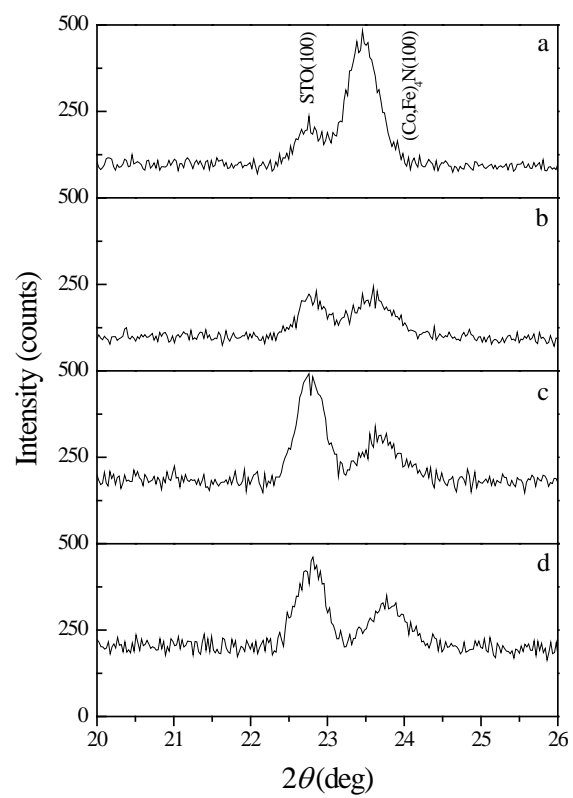


Fig. 3

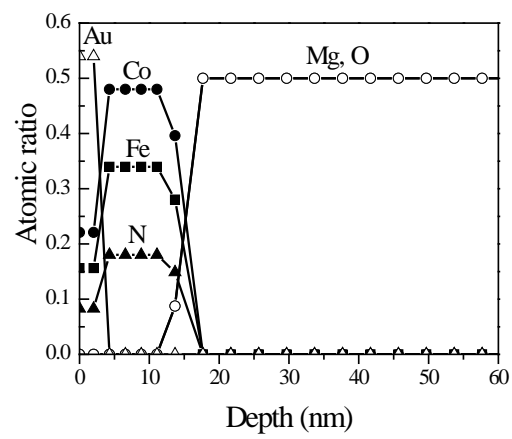


Fig. 4

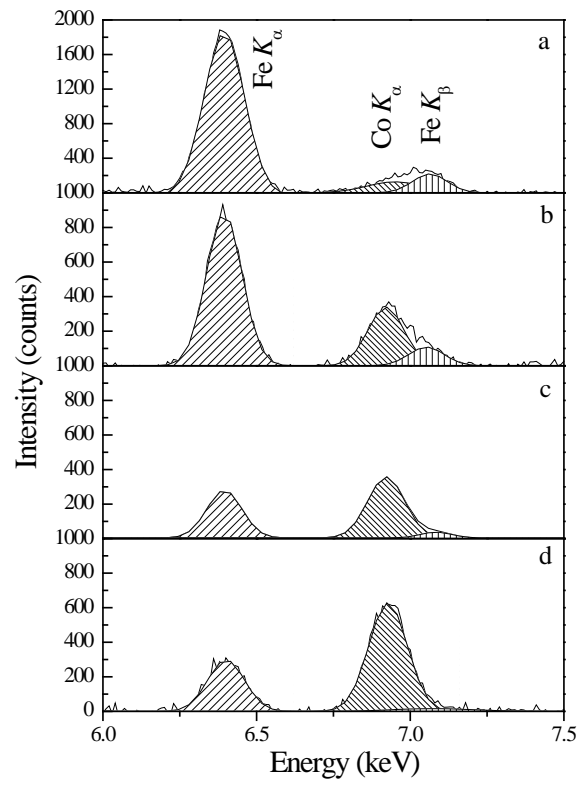
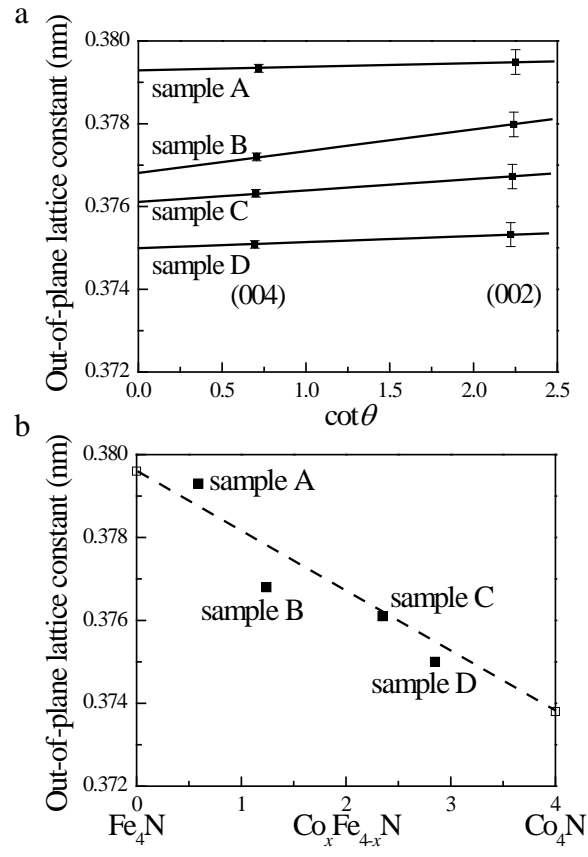
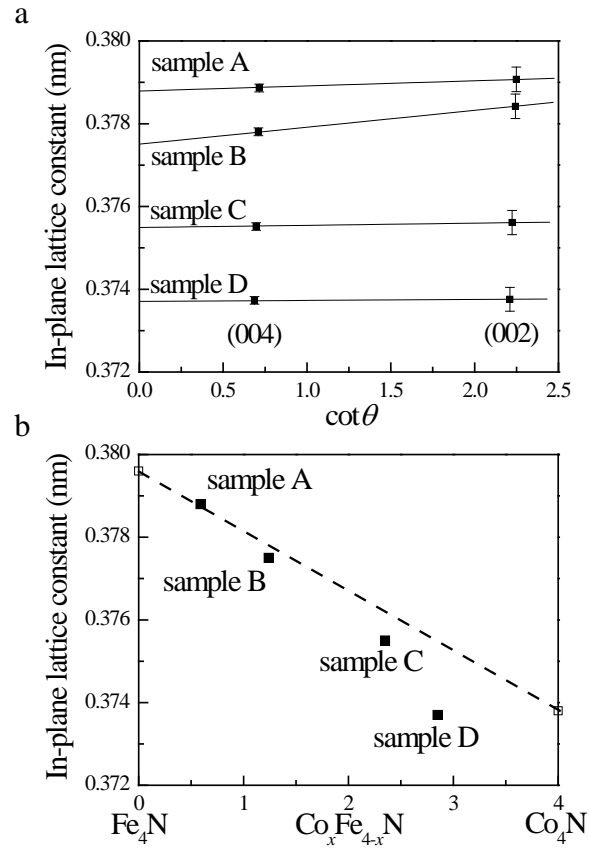


Fig. 5



Figs. 6



Figs. 7